Biosensors and Bioelectronics 42 (2013) 626–631

Contents lists available at SciVerse ScienceDirect

Biosensors and Bioelectronics

journal homepage: www.elsevier.com/locate/bios

Alkanethiol-functionalized terahertz metamaterial as label-free, highly-sensitive and specific biosensor

Xiaojun Wu [a], Baogang Quan [a], Xuecong Pan [a], Xinlong Xu [a,b,*], Xinchao Lu [c], Changzhi Gu [a], Li Wang [a]

[a] Beijing National Laboratory for Condensed Matter Physics and Institute of Physics, Chinese Academy of Sciences, Beijing 100190, China
[b] Nanobiophotonic Center, State Key Lab Incubation Base of Photoelectric Technology and Functional Materials, and Institute of Photonics & Photon-Technology, Northwest University, Xi'an 710069, China
[c] Institute of Microelectronics, Chinese Academy of Sciences, Beijing 100029, China

ARTICLE INFO

Article history:
Received 9 August 2012
Received in revised form
5 October 2012
Accepted 30 October 2012
Available online 7 November 2012

Keywords:
Biosensor
Biospecification
Metamaterial
Terahertz spectroscopy

ABSTRACT

Specific biorecognition is essential for many biological processes, for which highly sensitive and label-free biosensors are strongly demanded. The recently developed metamaterials are a potential choice for biosensing due to their exotic properties. In the current work, a label-free and specific sensor for streptavidin–agarose (SA) was fabricated based on terahertz metamaterial functionlized by octadecanthiols and biotins. Both low and high frequency resonant modes from the metamaterials are found applicable for the detection of SA, and a redshift up to 6.76 GHz for the high frequency mode was measured in the undiluted commercial solution. The low frequency mode is attributed to inductor–capacitor (LC) oscillation, while the high frequency mode originates from the plasmonic dipole oscillator, both of which are highly sensitive to the micro-environment change. Adsorption of SA of different concentrations causes different redshifts, and the replacement of high refractive-index substrate with low refractive-index substrate can efficiently promote the sensitivity, well agreeing with the numerical simulation. Moreover, for a particular biomolecule, the sensitivity can be further improved by optimizing the metamaterial design. This method might be very helpful for desirable biorecognition in biology, medicine, and drug industry.

1. Introduction

Specific interactions between molecules are the fundamental process for chemical analysis, medical diagnosis, environmental protection, food surveillance, and so on. Although labeling technique such as fluorescein based method (Kida et al., 2010) has played a significant role in the specific biomolecular interaction analysis, this labeling treatment may cause cross reaction between non-targeted molecules, which decreases the specificity of the assays and limits the sensitivity due to the background noise. Therefore, reliable, effective, and specific label-free biorecognition techniques are always highly demanded to enhance the signal discrimination.

Recently, metamaterials as a novel approach to control and manipulate electromagnetic wave have attracted wide attention in optical field. Understanding the light-metamaterial interaction mechanism is not only of fundamental significance for theory (Boltasseva and Atwater, 2011; Yanchuk et al., 2010) but also of interest for potential applications such as super-resolution imaging (Fang et al., 2005), perfect cloaking (Valentine et al., 2009; Schurig et al., 2006), and high-sensitivity detection (Chen et al., 2012; Tao et al., 2012). In the roadmap of metamaterial applications, sensing will be one of the next pleasant prospects. Sensors based on metamaterials have emerged from microwave (Dragoman et al., 2011; Yang et al., 2010), through far-infrared (Wu et al., 2012), to the visible band (Xu et al., 2011). It was found that the resonant modes from metamaterials are very sensitive to its micro-environment change (Driscoll et al., 2007). However, previous works focused mainly on the non-specific type of sensing with the measurand physically adsorbed to metamaterial sensors (Al-Naib et al., 2008), which demanded a large amount of analyte, but reduced the resolution. Moreover, such physical monitoring is not suitable for the specific biomolecular interaction analysis. In the cases of tracing analysis or minute concentration of analytes, such as cancer or tumor tissue diagnosis in the early stage (Lorenzo et al., 2012), a high-sensitivity and specific detection of metamaterial based sensors is desirable.

Even though the blooming in the optical sensors based on surface or localized plasmon resonance in visible region, the number of sensors operating in the far-infrared region, especially in terahertz (THz) region is relatively scarce. THz region is particularly promising in biosensor field due to the low photon energy and some specific

* Corresponding author at: Institute of Photonics & Photon-Technology, Northwest University, Xi'an 710069, China. Tel./fax: +86 29 88303336.
E-mail address: xlxuphy@nwu.edu.cn (X. Xu).

0956-5663/$ - see front matter © 2012 Elsevier B.V. All rights reserved.
http://dx.doi.org/10.1016/j.bios.2012.10.095

features (Brucherseifer et al., 2000; Menikh et al., 2004). For example, THz time-domain spectroscopy (THz-TDS) has been employed to detect skin cancer (Pickwell et al., 2004), distinguish drugs (Du et al., 2012), and characterize DNA (King and Korter, 2011), proteins (Sun et al., 2011) and some carbohydrates (Brown et al., 2007). Although many biological/chemical molecules have fingerprint signatures in THz region (Fischer et al., 2002; Brown et al., 2007; Walther et al., 2002) due to the inter- or intra-molecular vibrations, large sample quantity requirement, and strong absorption from water (Born et al., 2009; Heyden and Havenith, 2010; Jepsen et al., 2008) are still needed for special attention to overcome. Therefore, THz sensing based on waveguide (Nagel et al., 2002; Nagel and Kurz, 2006), high throughput microfluidic control systems (Laurette et al., 2010; Mendis et al., 2009), and also metamaterials (Sun et al., 2008), has evidenced a rapid development in the past few years.

One popular strategy to enhance the sensitivity of metamaterials is to optimize the structure parameters. For example, Debus et al. proposed asymmetric split ring resonators with sharp resonances as non-specific biosensors with the frequency shift of 4 GHz (Debus and Bolivar, 2007). However, specification can only be introduced by the functionalization. Functionalized (Tantakitti et al., 2012) metamaterials with alkanethiol molecules of well-ordered, covalent bonded monolayers afford a platform for further label-free sensing application (Lee et al., 2011; Lee and Yook, 2008). It might be feasible to realize a label-free biosensor, which can combine high sensitivity and selectivity with the functionalized metamaterials.

In this work, a label-free and specific biosensor for streptavidin–agarose (SA) was fabricated based on THz metamaterial functionlized by octadecanthiols and biotins. Both the low and high frequency resonant modes (LFRM & HFRM) from metamaterials are found applicable for the detection of SA, and a redshift up to 6.76 GHz for HFRM was observed with the commercial SA solution. Both modes are highly sensitive to the effective dielectric environment. Therefore, adsorption of SA with different concentration causes different redshifts and the replacement of substrates with low refractive index substrate results in high sensitivity, which was reproduced with the numerical simulation. Moreover, the sensitivity can be further optimized by metamaterial design for a particular biomolecule as necessary. This method might be very helpful for desirable biorecognition in biology, medicine, and drug industry.

2. Experimental

2.1. Metamaterial fabrication

Metamaterials with the periodic patterns of U-shaped golden split ring resonators (SRRs) were fabricated on both silicon (thickness of 500 μm, resistivity of 100 Ωcm) and quartz substrates (thickness of 800 μm) by conventional microfabrication techniques, including UV photolithography (MA6 UV photolithographer, Karl Süss Company, German), thermal evaporation (Sky Technology Development Co. Ltd., China), lift-off processes, and so on. In general, the silicon or quartz substrates were coated with S1813/LOR bilayer resists as sacrificial layers, firstly. Then the coated substrates were exposed by MA6 UV photolithographer. After the development, thin gold film was deposited on the coated substrates by the thermal evaporation method. Finally, a lift-off process was performed to wash out the sacrificial layers to form the designed metamaterials. The structural parameters are as follows: dimension of a SRR 31 μm (length=width=31 μm), the gap 5 μm, width of the line 3 μm, period 50 μm, and the thickness of Au 80 nm. The whole metamaterial pattern can reach an area of 1 cm × 1 cm. The scanning electron microscopy (SEM) micrographs of the SRRs are illustrated in Fig. 1. Oxygen plasma treatment for ten minutes is adopted to remove organic contamination before they are functionalized.

2.2. Chemicals and materials

Octadecanthiol (ODT, $CH_3(CH_2)_{17}SH$) was purchased from Sigma–Aldrich (Shanghai, China). Biotin (CAS Number 58-85-5) was purchased from Sinopharm Chemical Reagent Co. Ltd. (Beijing, China). Phosphate buffer solution (PH 7.4 BIOREA) was purchased from Sigma–Aldrich (Shanghai, China). SA with the

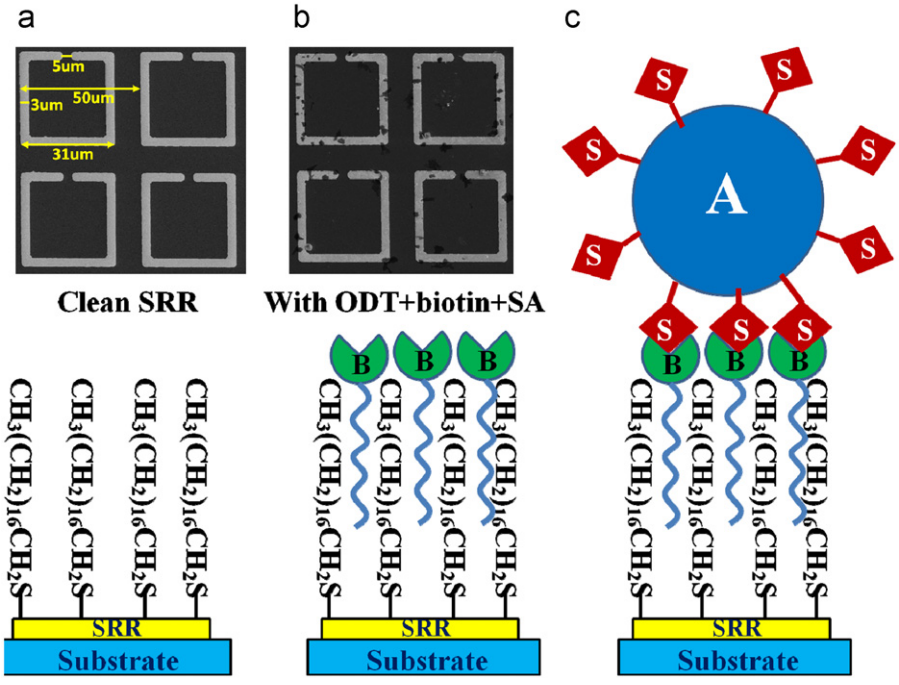

Fig. 1. Schematic diagram of (a) ODT (7 mM) functionalization of SRRs surfaces; (b) biotinylation (0.5 mg/ml) on ODT; (c) specific biorecognization of SA. Top-left shows the SEM of SRRs without and with biomolecules for comparison.

characteristics as follows: extent of labeling ≥1 mg per ml; matrix 4% beaded agarose; capacity ≥15 μg/ml binding capacity. It was also purchased from Sigma–Aldrich (Shanghai, China). Lactose was purchased from ZhongKeChenYu Biotech Co. Ltd (Beijing, China). All other chemicals such as ethanol were analytical grade and all stock and buffer solutions were prepared with autoclaved doubly distilled water (DDW).

2.3. Functionalization and sensor preparation

The metamaterial based sensors were prepared with the functionalization of ODT followed by the immobilization of biotin. Firstly, sensor chips were immersed in the ethanol solution of ODT at a concentration of 7 mM, for 16 h at room temperature to obtain well aligned, tightly bonded self-assemblage on the gold surface (Cismaru et al., 2012; Rouhana et al., 2011). Then the ODT functionalized sensor chips were washed thoroughly by ethanol and dried by nitrogen. Furthermore, the gold surface of the metamaterials was covered by a droplet (50 μl) of 0.5 mg/ml biotin dissolved in DDW, and sealed for 2 h. The spontaneous immobilization of biotin into ODT self-assemblage guarantees the stability of the ODT-biotin complex. The SRRs surfaces were repeatedly washed with a phosphate buffer solution (pH 7.4) to eliminate the non-specific bonded molecules. After dried under a stream of nitrogen, a droplet (50 μl) of SA solution was dripped to completely cover the gold surface of SRRs, and again sealed for 2 h. Five samples of different concentrations, specified as volume ratio SA:DDW (sample Number #1: 10 μl: 40 μl; #2: 20 μl: 30 μl; #3: 30 μl: 20 μl; #4: 40 μl: 10 μl; #5: 50 μl: 0 μl) were prepared. That covered by 11.5 mg/ml lactose solution (50 μl) for 2 h, numbered as #0, was used as control sample. All the aforementioned surface functionalization and modification were schematically illustrated in Fig. 1.

In general, the gold-based metamaterial surface is functionalized via specific thiol chemical interaction to form a monolayer of thiol-terminated molecules. The intermolecular interaction between the alkyl chain of the thiol and biotin immobilizes the biotin onto the metamaterial surface. As an affinity effect, the biotin will have a specific interaction with the SA. Two SEM micrographs in Fig. 1 display four clean and four functionalized SRRs for comparison. The black spots on the surface of the right side SRRs are the aggregation of biotin and SA molecules.

2.4. THz-TDS setup

The experiments were conducted with a custom-designed assembled THz-TDS system as shown in Fig. 2. A Ti:Sapphire femtosecond laser (Maitai Spectra-Physics, 80 MHz repetition rate, 70 fs pulse width) is divided into two beams. The one with an average power of ~30 mW is used to generate THz pulses while the other is used as probing beam. The excitation beam passes through a delay stage, a chopper and is then focused onto a low-temperature grown GaAs photoconductive antenna (Zomega Terahertz Corp., 50 μm gold gap, 80 V AC voltage) integrated with a silicon hemisphere lens. The generated THz pulses are aligned by two off-axis paraboloidal mirrors and then focused onto the sample. The transmitted THz pulses are further aligned by another two off-axis paraboloidal mirrors and focused onto the 〈110〉 ZnTe detector, together with the probing pulses, which are reflected by a high resistance silicon wafer of 0.5 mm in thickness. The refractive index of the detecting crystal is modulated by the presence of the THz electric field. According to linear electro-optical effect (Pockels effect), the THz electric field is detected indirectly by the intensity variation of the polarization state of the probe beam. The modulated probing light goes through a quarter wave plate and a Wollaston prism, finally arrives at a pair of balance photodiodes. The differential photocurrent between the two photodiodes is guided to a lock-in amplifier. This coherent detection method can take the time-domain THz pulse wave and after fast Fourier transformation, we can extract both the amplitude and phase of the transmitted THz electromagnetic wave through the samples. The propagation path for the THz wave is sealed and filled with nitrogen to avoid absorption by water vapor. The dynamic range of our system, defined as the maximum value of the THz temporal waveforms divided by the maximum of the background noise, is about 10,000.

3. Results

Compared with the conventional sensors, metamaterial-based sensors have a higher degree of design freedom. For example, we have studied the influence of substrate and metal properties on the inductor–capacitor (LC) oscillating response of metamaterials in THz region and have found that proper substrates and metals choose can shift the resonant peaks to the desired modes (Xia et al., 2008). Fig. 3 demonstrated further that different substrates would also have different sensitivity for metamaterial-based sensors. The THz transmission spectra of metamaterials, with and without biomolecules, fabricated on (a) silicon and (b) quartz is shown in Fig. 3. The polarization of the wave was aligned along the U-shaped SRRs gap. The samples with biomolecules were prepared with the same concentration of ODT, biotin and SA:DDW (50 μl:0 μl). It is obvious that there exist two sharp resonant transmission minima. The low frequency resonant mode (LFRM) are located at ~0.4 THz and the high frequency resonant mode (HFRM) at ~1.2 THz for SRRs on silicon, while on quartz the LFRM shifts to ~0.75 THz and the HFRM shifts to ~2.0 THz, respectively.

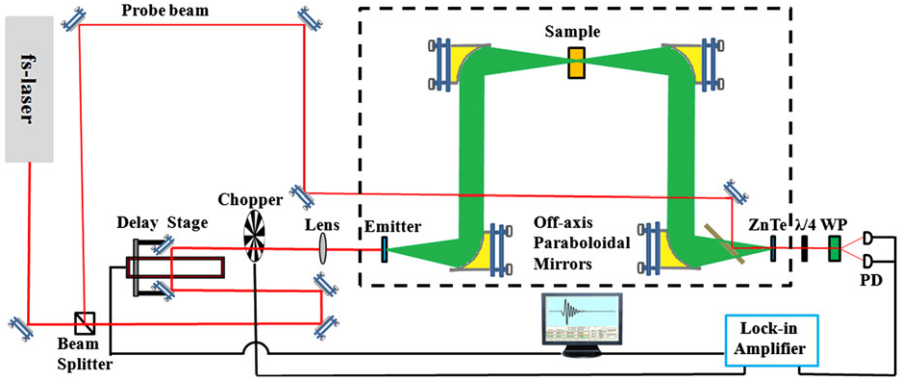

Fig. 2. Schematic setup of the custom-designed assembled THz time-domain spectrometer.

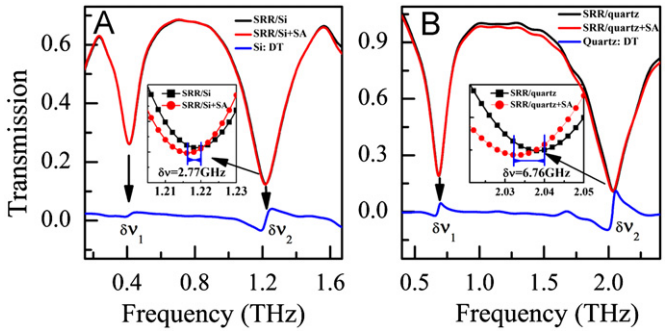

Fig. 3. THz transmission of SRRs on silicon (a) and on quartz (b) with (red line) and without (black line) biomolecules. The inset shows the zoomed frequency shift of high frequency resonant mode with (red circle) and without (black square) non-diluted SA solution. Also the curves for the differential transmission normalized to that of the sample without molecules, is presented (blue line). (For interpretation of the references to color in this figure legend, the reader is referred to the web version of this article.)

In order to accentuate the molecular modification effect, the differential transmission of SRRs with and without molecules $(T_{with}-T_{without})/T_{without}$ is shown in Fig. 3 (blue line), where the features with a derivative of the Lorentzian profile is ready to be identified. It should be noticed that the frequency redshift becomes more obvious for HFRM. For example, HFRM shifts about 2.77 GHz in (a) while in (b) it amounts to 6.76 GHz. Similar results can also be observed for the LFRM, where it shifts ~0.75 GHz on silicon while ~1.58 GHz on quartz. This suggests that the sensitivity can be dramatically enhanced simply by replacing the silicon substrate (the refractive index n of ~3.4) with quartz (n of ~2.0). To our best knowledge, the redshift of 6.76 GHz is the biggest modulation of metamaterial biosensors with a monolayer biomolecules reported in THz band. The higher redshift could come from two reasons. Firstly, it is from the optimization of the substrate, which shows the effect of lower dielectric constant of substrate for higher redshift as discussed later. The other reason could come from special optical properties of metamaterials with the strong electrical field enhancement in the gap of SRRs.

The interaction between SA and biotin is a dynamical balance during the specific biorecognition, when the functionalized metamaterials are immersed into the SA solution. Different concentration of SA will have variable mount of SA binding to functionalized metamaterials, which can be used to further clarify the sensitivity of the SRRs biosensor. Fig. 4 illustrates the frequency redshifts of the HFRM and LFRM on quartz as a function of the sample number as discussed above, which is in positive correlation with the SA concentration. In the concerned concentration range in Fig. 4, the redshift value increases with the increasing of SA concentration. The control experiment conducted with the high concentration of lactose solution (less non-specific binding to biotin) shows a redshift of less than 1.0 GHz for HFRM. However, for the high affinity of SA and biotin, a redshift for ~1.06 GHz was measured for the lowest concentration, which can be discriminate against the control sample. As for the LFRM, the frequency redshift for the lowest concentration is ~0.22 GHz, whereas it is only ~0.04 GHz for the control sample. Numerical simulation using finite integral technique is employed to simulate the effect of micro-environmental dielectric change of substrate and analyte layers. Due to the compuational complexity (Wu. and Iwamoto, 1997), the SA molecule coating on the U-shaped gold SRRs was treated as a layer in the scale of micrometer (2 μm) in thickness instead of the nanometer scale and the permittivity was set to 1.2 (Xia et al., 2008). With the additional biomolecular layer on top of the sensor, the simulated results give the redshift of both resonant modes, with the HFRM more sensitive than LFRM, which agree well with the experiments. With the increasing of the

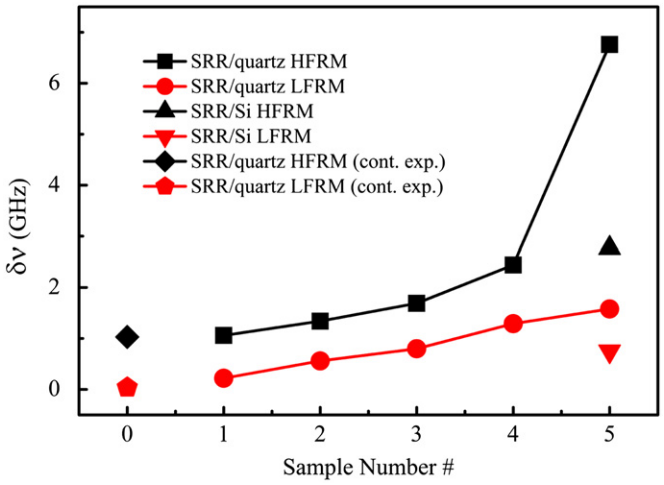

Fig. 4. Frequency shift of SRRs on quartz with five different volume ratio of SA:DDW: #0: no SA; #1: 10 μl:40 μl; #2: 20 μl:30 μl; #3: 30 μl:20 μl; #4: 40 μl:10 μl; #5: 50 μl:0 μl. The results obtained from samples on silicon substrate, with the largest SA concentration, and control experiment are also presented for comparison.

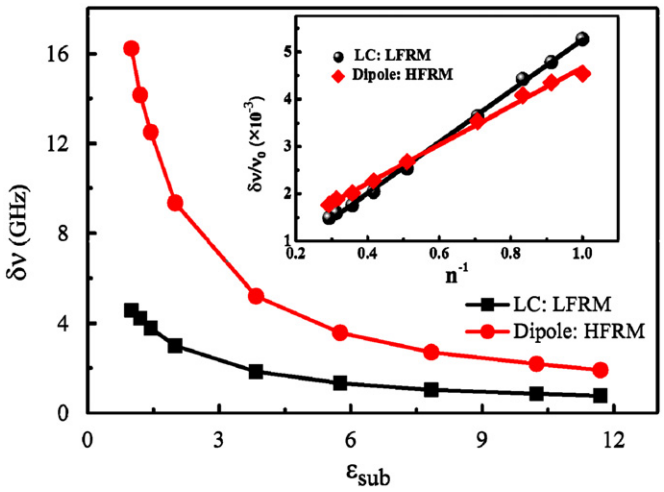

Fig. 5. Numerical simulation of the sensitivity dependence of substrate permittivity. Insert shows a linear relationship of normalized frequency shift with the reciprocal of refractive index of the substrate.

permittivity (ε) of the substrate, both resonant modes shift to lower frequency, as shown in Fig. 5. The frequency shifts demonstrate a nonlinear decay with the increase of substrate permittivity. The HFRM shifts much more than the LFRM, which agrees well with the experimental results. In particular, the redshift of 5.4 GHz for silicon (ε=11.56) and 9.5 GHz for quartz (ε=4.0), which roughly reproduce the experimental results.

4. Discussion

From the LC resonance point of view, the LFRM can be explained by a combination of capacitance and inductance. The eigenfrequency is given as $\omega_{LC}=(LC)^{-1/2}$, where the inductance L is determined mainly by the geometry of the SRRs and the capacitance C depends on both the gap dimension and the medium (Padilla et al., 2006). This LC resonator mainly induces the artificial magnetic response in THz region when the polarization of THz wave is along the SRRs gap. Usually the inductance in a single SRRs or the mutual inductance between SRRs are quite inertia to the environmental

change, while the capacitance show more sensitive to the environmental change (Sun et al., 2008). Similar to Hara's suggestion (Hara et al., 2008), the total functionalized SRRs capacitance ($C=C_1+C_2+C_3+C_4+C_5$) can be modeled as five parallel capacitors: the capacitance due to flux within the substrate (C_1), capacitance due to fringing flux between substrate and SRRs (C_2), capacitance due to flux within the gap of SRRs (C_3), capacitance due to the flux within the SA (C_4), and capacitance due to fringing flux between SRRs and SA (C_5). With the increasing of ambient dielectric near SRRs, the total capacitance will increase, resulting in the redshift of the LFRM.

HFRM, on the other hand, is suggested by Pendry et al. (1999) as a diluted plasmonic resonance, which can be approximately described by a plasmonic dipole resonant frequency at $\omega\sim 1/(2d\varepsilon_{eff}^{1/2})$ (Padilla et al., 2006), where d is the length of the SRRs arms and ε_{eff} is the average dielectric constant of the surrounding medium as $\varepsilon_{eff}=\varepsilon_{sub}+\Phi\varepsilon_{air}+(1-\Phi)\varepsilon_{SA}$. Where, Φ is the fraction filled by air. ε_{sub}, $\Phi\varepsilon_{air}$ and ε_{SA} are the dielectric constant of the substrate, air and SA, respectively. When biomolecules bond to the gold surface of the SRRs, ε_{eff} would increase, which results in the redshift of HFRM (Romaner et al., 2008). In microscopic view, the adoption of SA will also cause a stronger depolarization field around the SRRs, which will restrict the driven movement of electrons in the SRRs (Alloway et al., 2003), and the conductivity of gold would also decrease when the sulfur bond to it (Rouhana et al., 2011). All of aforementioned factors may introduce the redshift of the HFRM.

The different origins of LFRM and HFRM show different sensitivity as application. With the adsorption of SA to SRRs (Fig. 2), the mainly capacitance change is $C4$ and $C5$, and the modulation of total capacitance C is relative to the ratio of $(C4+C5)/(C1+C2+C3+C4+C5)$. $C4$ and $C5$ (considering as micro-parallel plates capacitor as a function of $\varepsilon d/s$, with ε dielectric, d thickness, s the area) change is relatively small compared to the total capacitance, which is due to the nanometer scale of monolayer compared with THz wave length, resulting in a small redshift of the LFRM. However, HFRM arises from the dipole resonant characteristic $1/(2d\varepsilon_{eff}^{1/2})$, which is mainly related to the micro-environment dielectric change. Unlike the LFRM, the HFRM have the plasmonic resonant characteristic, which could be resonantly enhanced to the bonded inter- or intra-molecular vibrations in THz and far-infrared region (Cubukcu et al., 2009), resulting in much larger redshift.

The interaction between SA and biotin is a dynamical balance in SA solution with a dissociation constant on the order of $\sim 10^{-14}$ mol/L. The SA solution with higher concentration gets a greater chance to affinity interaction with biotin, resulting in a larger modulation of micro-environmental dielectric change and a larger frequency shift (Jung and Campbell (2000)) as shown in Fig. 4. The sensing of these nanometer monolayer molecules with THz wave (wavelength in the scale of micrometer) would be challengeable without the help of functionalized metamaterials. Menikh et al. (Menikh et al., 2004) developed another THz wave technology called doubled-modulated THz differential TDS (THz-DTDS) for the bioaffinity monitoring of monolayer between biotin and avidin. Our approach is much simpler and more easily to implement compared with the THz-DTDS.

Even though we know substrate effect for metamaterials based sensors, a suitable relationship between the sensitivity and the dielectric of substrate needed further understood. We redrawn the frequency shift δv normalized to resonant frequency v_0 in Fig. 5 as a function of the reciprocal of refractive index (n) (inserted in Fig. 5). We found that a good linearity of $\delta v/v_0=A+B/n$ (A, B are parameters). This relationship suggested that high dielectric constant substrate has a limitation to the sensitivity, while free-standing metamaterials would be the highest sensitive biosensor, even though it is difficult to fabricate. This relationship is also very useful for us to choose the proper substrate and to evaluate the frequency shift when we change the substrate.

Through monitoring the resonant mode shift of the functionalized THz metamaterials, metamaterial based sensors have some advantages compared with the conventional surface plasmon resonance biosensors. For example, it does not need any prisms or gratings for coupling the incident light, which allows a very convenient operation. Moreover, many biomolecules, such as DNA or protein have resonant vibration or rotation modes in THz region, which can be selectively resonant with the designed THz metamaterial towards a highly boosted sensitivity (Wu et al., 2012). This technique might be helpful to resolve the conformational variations of biomolecules under varying environment (Wu et al., 2012; Cubukcu et al., 2009).

5. Conclusion

In summary, we demonstrated a highly-sensitive, label-free and specific biosensor to recognize SA, based on THz metamaterials functionlized by octadecanthiol, followed with biotinylation. With a metamaterial structure fabricated on quartz, a frequency redshift as high as 6.76 GHz was measured for the HFRM with the commercial non-diluted SA concentration. We found a linear relationship of normalized frequency shift with the reciprocal of refractive index of the substrate. Moreover, the sensitivity can be further optimized by metamaterial design for a particular biomolecule as necessary. This emergent field offers another promising platform for sensing with the characteristics of designable and tunable resonant features. As a young research field, more real bio-systems and applications are desirable and will be developed. Ongoing research such as monitoring the interaction between lambda-DNA and anticancer drug oxaliplatin with metamaterials, are undertaken in our lab. This method might be very helpful for desirable biorecognition in biology, medicine, and drug industry.

Acknowledgments

This work is supported by National Natural Science Foundation of China (Grant Nos. 10834015, 61077082, 51103175), Natural Science Basic Research Plan in Shaanxi Province of China (Grant No. 2012KJXX-27). Dr. Xu acknowledges support from the open foundation of State Key Lab Incubation Base of Photoelectric Technology and Functional Materials (No. ZS12018).

References

Alloway, D.M., Hofmann, M., Smith, D.L., Gruhn, N.E., Graham, A.L., Colorado Jr., R., Wysocki, V.H., Lee, T.R., Lee, P.A., Armstrong, N.R., 2003. The Journal of Physical Chemistry B 107 (42), 11690–11699.
Al-Naib, I.A.I., Jansen, C., Koch, M., 2008. Applied Physics Letters 93 (8), 083507.
Born, B., Weingartner, H., Bründermann, E., Havenith, M., 2009. Journal of the American Chemical Society 131 (10), 3752–3755.
Boltasseva, A., Atwater, H.A., 2011. Science 331 (6015), 290–291.
Brown, E.R., Bjarnason, J.E., Fedor, A.M., Korter, T.M., 2007. Applied Physics Letters 90 (6), 061908.
Brucherseifer, M., Nagel, M., Bolivar, P.H., Kurz, H., Bosserhoff, A., Buttner, R., 2000. Applied Physics Letters 77 (24), 4049–4051.
Chen, T., Li, S., Sun, H., 2012. Sensors 12 (3), 2742–2765.
Cismaru, A., Dragoman, M., Radoi, A., Dinescu, A., Dragoman, D., 2012. Journal of Applied Physics 111 (7), 076106.
Cubukcu, E., Zhang, S., Park, Y.-S., Bartal, G., Zhang, X., 2009. Applied Physics Letters 95 (4), 043113.
Debus, C., Bolivar, P.H., 2007. Applied Physics Letters 91 (18), 184102.
Dragoman, M., Cismaru, A., Radoi, A., Voicu, M., Dragoman, D., 2011. Applied Physics Letters 99 (25), 253106.
Driscoll, T., Andreev, G.O., Basov, D.N., Palit, S., Cho, S.Y., Jokerst, N.M., Smith, D.R., 2007. Applied Physics Letters 91 (6), 062511.

Du, S.Q., Li, H., Xie, L., Chen, L., Peng, Y., Zhu, Y.M., Dong, P., Wang, J.T., 2012. Applied Physics Letters 100 (14), 143702.
Fang, N., Lee, H., Sun, C., Zhang, X., 2005. Science 308 (5721), 534–537.
Fischer, B.M., Walther, M., Jepsen, P.U., 2002. Physics in Medicine and Biology 47 (21), 3807–3814.
Heyden, M., Havenith, M., 2010. Methods 52 (1), 74–83.
Jepsen, P.U., Jensen, J.K., Moller, U., 2008. Optics Express 16 (13), 9318–9331.
Jung, L.S., Campbell, C.T., 2000. Physical Review Letters 84 (22), 5164–5167.
Kida, N., Katsuda, Y., Yoshikawa, Y., Komeda, S., Sato, T., Saito, Y., Chikuma, M., Suzuki, M., Imanaka, T., Yoshikawa, K., 2010. Journal of Biological Inorganic Chemistry 15 (5), 701–707.
King, M.D., Korter, T.M., 2011. The Journal of Physical Chemistry A 115 (50), 14391–14396.
Laurette, S., Treizebre, A., Affouard, F., Bocquet, B., 2010. Applied Physics Letters 97 (11), 111904.
Lee, H.-J., Lee, J.-H., Jung, H.-I., 2011. Applied Physics Letters 99 (16), 163703.
Lee, H.-J., Yook, J.-G., 2008. Applied Physics Letters 92 (25), 254103.
Lorenzo, L.R., Rica, R. d.l.., Álvarez-Puebla, R.A., Liz-Marzán, L.M., Stevens, M.M., 2012. Nature Materials 11 (7), 604–607.
Mendis, R., Astley, V., Liu, J., Mittleman, D.M., 2009. Applied Physics Letters 95 (17), 171113.
Menikh, A., Mickan, S.P., Liu, H.B., MacColl, R., Zhang, X.C., 2004. Biosensors and Bioelectronics 20 (3), 658–662.
Nagel, M., Bolivar, P.H., Brucherseifer, M., Kurz, H., Bosserhoff, A., Buttner, R., 2002. Applied Optics 41 (10), 2074–2078.
Nagel, M., Kurz, H., 2006. International Journal of Infrared and Millimeter Waves 27 (4), 517–529.
O'Hara, J.F., Singh, R., Brener, I., Smirnova, E., Han, J.F., Taylor, A., Zhang, W.L, 2008. Optics Express 16 (3), 1786–1795.
Padilla, W.J., Taylor, A.J., Averitt, R.D., 2006. Physical Review Letters 96 (10), 107401.
Pendry, J.B., Holden, A.J., Robbins, D.J., Stewart, W.J., 1999. IEEE Transactions on Microwave Theory and Techniques 47 (11), 2075–2084.
Pickwell, E., Cole, B.E., Fitzgerald, A.J., Pepper, M., Wallace, V.P., 2004. Physics in Medicine and Biology 49 (9), 1595–1607.
Romaner, L., Heimel, G., Ambrosch-Draxl, C., Zojer, E., 2008. Advanced Functional Materials 18 (24), 3999–4006.
Rouhana, L.L., Moussallem, M.D., Schlenoff, J.B., 2011. Journal of the American Chemical Society 133 (40), 16080–16091.
Schurig, D., Mock, J.J., Justice, B.J., Cummer, S.A., Pendry, J.B., Starr, A.F., Smith, D.R., 2006. Science 314 (5801), 977–980.
Sun, Y., Xia, X., Feng, H., Yang, H., Gu, C., Wang, L., 2008. Applied Physics Letters 92 (22), 221101.
Sun, Y.W., Zhang, Y.T., Pickwell-MacPherson, E., 2011. Biophysical Journal 100 (1), 225–231.
Tantakitti, F., Burk-Rafel, J., Cheng, F., Egnatchik, R., Owen, T., Hoffman, M., Weiss, D.N., Ratner, D.M., 2012. Langmuir 28 (17), 6950–6959.
Tao, H., Brenckle, M.A., Yang, M., Zhang, J., Liu, M., Siebert, S.M., Averitt, R.D., Mannoor, M.S., McAlpine, M.C., Rogers, J.A., Kaplan, D.L., Omenetto, F.G., 2012. Advanced Materials 24 (8), 1067–1072.
Valentine, J., Li, J., Zentgraf, T., Bartal, G., Zhang, X., 2009. Nature Materials 8 (7), 568–571.
Walther, M., Plochocka, P., Fischer, B., Helm, H., Jepsen, P.U., 2002. Biopolymers 67 (4-5), 310–313.
Wu, C., Khanikaev, A.B., Adato, R., Arju, N., Yanik, A.A., Altug, H., 2012. Nature Materials 11 (1), 69–75.
Wu., C.X., Iwamoto, M., 1997. Physical Review B 55 (16), 10922–10930.
Xia, X., Sun, Y., Yang, H., Feng, H., Wang, L., Gu, C., 2008. Journal of Applied Physics 104 (3), 033505.
Xu, X., Peng, B., Li, D., Zhang, J., Wong, L.M., Zhang, Q., Wang, S., Xiong, Q., 2011. Nano Letters 11 (8), 3232–3238.
Yanchuk, B.L., Zheludev, N.I., Maier, S.A., Halas, N.J., Nordlander, P., Giessen, H., Chong, C.T., 2010. Nature Materials 9 (9), 702–715.
Yang, J., Huang, M., Xiao, Z., Peng, J.H., 2010. Modern Physics Letters B 24 (12), 1207–1215.